Journal of Catalysis **181,** 91–103 (1999)
Article ID jcat.1998.2286, available online at http://www.idealibrary.com on IDEAL®

Studies on Carbon Deposition in CO_2 Reforming of CH_4 over Nickel–Magnesia Solid Solution Catalysts

Keiichi Tomishige,[1] Yang-guang Chen, and Kaoru Fujimoto

Department of Applied Chemistry, School of Engineering, The University of Tokyo, Hongo 7-3-1, Bunkyo-ku, Tokyo 113-8656, Japan
E-mail: tomi@hongo.ecc.u-tokyo.ac.jp

Received May 18, 1998; revised September 16, 1998; accepted September 23, 1998

Carbon formation behavior under CH_4-CO_2 reaction and through CH_4 decomposition and CO disproportionation was investigated over $Ni_{0.03}Mg_{0.97}O$ solid solution, supported Ni/MgO, and NiO-Al_2O_3 catalysts by means of thermogravimetric analysis (TGA) and transmission electron microscopy (TEM). $Ni_{0.03}Mg_{0.97}O$ showed high resistance to carbon formation in CO_2 reforming of methane and the selectivity to carbon formation was much lower than two other catalysts. It is suggested that CO_2 plays an important role in the inhibition of carbon formation on $Ni_{0.03}Mg_{0.97}O$ through the activation of CO_2 at the interface between small nickel particles and the support surface.

Key Words: **carbon deposition; CO_2 reforming of CH_4; nickel–magnesia solid solution catalyst; thermogravimetric analysis; whisker carbon.**

INTRODUCTION

Catalytic reforming of CH_4 with CO_2 to produce synthesis gas has gained a growing interest in the last two decades, considering the chemical utilization of natural gas and CO_2, which are substances intimately related to the environment and energy resources (1, 2). Natural gas, whose main component is methane, is known to have a reserve comparable to that of petroleum, while carbon dioxide is a greenhouse gas. So far, the most promising process for the chemical utilization of natural gas is its conversion to liquid fuels or valuable oxygenated chemicals via synthesis gas, which is conventionally produced by the steam reforming of CH_4 (3).

$$CH_4 + H_2O \rightarrow CO + 3H_2 \quad (\Delta H_{298} = +206 \text{ kJ/mol}). \quad [1]$$

This reaction is industrially operated under reaction temperature of 1000–1130 K, total pressure of 2–4 MPa, and the ratio of partial pressure of $H_2O/CH_4 = 2$–6. The use of excess H_2O in the reactant gas is to inhibit the carbon deposition. Thermodynamically, the limitation of carbon deposition can be estimated by the H/C and O/C atomic ratios in the reactant gas (3). When the atomic ratio of H/C and O/C is higher, the amount of carbon deposition becomes less. However, the presence of excess H_2O favors the successive water–gas shift reaction (Eq. [2]) and, therefore, results in the product gas with H_2/CO ratio higher than 3:

$$CO + H_2O \rightarrow CO_2 + H_2 \quad (\Delta H_{298} = -41 \text{ kJ/mol}). \quad [2]$$

This is suitable for hydrogen production, but not desirable for the production of liquid hydrocarbons. The major commercial interest in the catalytic reforming of CH_4 with CO_2 (Eq. [3]) originates from this demand, since this reaction gives synthesis gas with a low H_2/CO ratio. On the other hand, there are some natural gas fields containing considerable amounts of CO_2 (4). In this case, it would be convenient for this reaction to be performed at this kind of natural gas field:

$$CH_4 + CO_2 \rightarrow 2CO + 2H_2 \quad (\Delta H_{298} = +247 \text{ kJ/mol}). \quad [3]$$

A number of studies have been focused on the development of a catalytst for this reaction (5–19). It has been pointed out that the most serious problem is carbon deposition, which causes catalyst deactivation, plugging of the reactor, and breakdown of the catalyst (20, 21). Carbon deposition has also been observed in steam reforming of hydrocarbons. It has been reported that deposited carbon is formed via different routes, each influencing the morphology of the carbon. The most common types are whisker-like carbon, encapsulating carbon, and pyrolytic carbon (3). Methane decomposition (Eq. [4]) and CO disproportionation (Eq. [5]) are the main routes of the carbon formation:

$$CH_4 \rightarrow 2H_2 + C \quad (\Delta H_{298} = +75 \text{ kJ/mol}) \quad [4]$$

$$2CO \rightarrow CO_2 + C \quad (\Delta H_{298} = -173 \text{ kJ/mol}). \quad [5]$$

According to thermodynamic calculation, CO_2 reforming of CH_4 is much more prone to cause carbon deposition than steam reforming because of its low H/C ratio in the reactant gas. In addition, carbon deposition seems to be

[1] To whom correspondence should be addressed.

0021-9517/99 $30.00

unavoidable even under higher CO_2/CH_4 pressure ratios. Thus, the catalysts for steam reforming are not applicable to CO_2 reforming. This forces us to develop new catalysts. To suppress carbon deposition, some noble metals such as Rh and Ru are better to use as the active component than Ni, although Ni has activity comparable to noble metals (8, 15, 16, 19). However, considering the high cost and limited availability of these noble metals, it is more attractive to develop a nickel catalyst with high catalytic performance. It has been reported that basic oxide supports are effective for the inhibition of carbon deposition (22, 23). Some supported nickel catalysts have shown promising activity and long life without obvious deactivation (17, 22, 24). Recently, we found that an excellent one is a nickel magnesia solid solution catalyst, $Ni_{0.03}Mg_{0.97}O$ (22, 25, 26). After reduction at high temperature (~1123 K), it exhibited very high and stable activity without coke formation in both CO_2 reforming of CH_4 and steam reforming of CH_4 under $H_2O/CH_4 = 1$, where a large amount of carbon was deposited on the commercial steam reforming catalyst (26). Characterization results revealed that $Ni_{0.03}Mg_{0.97}O$ solid solution catalyst has highly dispersed nickel metal particles after reduction which interact with the support surface (27, 28).

In this paper, the carbon formation rates for CH_4-CO_2 reforming, CH_4 decomposition, and CO disproportionation were investigated, respectively, by means of thermogravimetry. We also examined the influence of the catalyst properties on carbon deposition by comparing the $Ni_{0.03}Mg_{0.97}O$ solid solution catalyst, the supported Ni/MgO catalyst, and the NiO-Al_2O_3 catalyst. Transmission electron microscopy, the measurement of H_2 and O_2 adsorption, XRD, and FTIR were performed to characterize these catalysts. The proposed carbon formation mechanism by this study will help to design an excellent catalyst with both long catalyst life and high resistance to carbon deposition.

EXPERIMENTAL

Catalyst Preparation

The $Ni_{0.03}Mg_{0.97}O$ solid solution catalyst was prepared by coprecipitating nickel acetate (>98.0%, Kanto Chemical Co., Inc.) and magnesium nitrate (>99.2%, Kanto Chemical Co., Inc.) aqueous solutions with potassium carbonate (>99.5%, Kanto Chemical Co., Inc.) aqueous solution. After being filtered and washed with hot water, the precipitate was dried overnight at 393 K and then calcined in air at 1223 K for 10 h in order to form a solid solution. And this was confirmed by XRD spectra. The same preparation method was also applied to the NiO-Al_2O_3 catalyst, in which magnesium nitrate was substituted by aluminum nitrate. The Ni/MgO supported catalyst was prepared by impregnating a home-made MgO support, of which the preparation method and condition were the same as those for the nickel–magnesia solid solution, with the acetone solution of nickel acetylacetonate complex (>99%, Soekawa) followed by drying at 393 K overnight. The Ni/MgO supported catalyst was not calcined at a high temperature because calcination at a high temperature makes the catalyst a solid solution. Before use, all these catalysts were pressed into tablets and crushed to 20–40 mesh of particles. The content of nickel in these three catalysts is $Ni/(Ni + M) = 0.03$ (M = Mg or Al). The catalysts were represented as $Ni_{0.03}Mg_{0.97}O$, 3 mol% Ni/MgO and NiO-Al_2O_3 (3 mol%).

Catalytic CH_4-CO_2 Reforming

Activity tests were carried out in a fixed-bed continuous-flow reactor made of 6-mm ID quartz tube. The amount of catalyst was 0.05 g. After the catalysts were reduced in flowing H_2 (99.9995%, Takachiho Trading Co., Ltd.) at 1123 K for 0.5 h, the reactant gas, which consisted of an equimolar mixture of CH_4 (99.99%, Takachiho Trading Co., Ltd.) and CO_2 (99.99%, Takachiho Trading Co., Ltd.), was introduced into the reactor under the reaction conditions of atmospheric pressure, 773 K, and W/F = 0.1 gh/mol. The effluent gas was analyzed with an on-line TCD gas chromatograph using 2 m of active carbon as the separating column. An ice bath was set between the reactor exit and the GC sampling valve to remove the water.

Thermogravimetric Studies

Thermogravimetric studies were performed by using TGD-7600 (ULVAC, Shinku-riko, Inc.). We used a quartz basket with 6-mm ID as the sample holder. The partial pressure of the reactant gas was $CH_4/N_2 = 25/75$ for methane decomposition, $CO/N_2 = 25/75$ for CO disproportionation, and $CH_4/CO_2/N_2 = 25/25/50$ for CO_2 reforming of CH_4. In each case, the catalyst weight was about 0.1 g and the total flow rate was 80 ml/min. The catalyst pretreatment involved two steps: first, the catalyst was reduced in pure H_2 flow at 1123 K for 30 min in a fixed bed continuous-flow reactor and then it was transferred to the thermogravimetric system under atmosphere; finally, the catalyst was re-reduced *in situ* with a 5% H_2/He flow at 1123 K for another 30 min. The temperature was raised at a heating rate of 20 K/min from room temperature to 1123 K. After this, the sample was cooled down to reaction temperature under nitrogen flow for purging the system. At the reaction temperature, the reactant gas was introduced and the change of weight was monitored at constant reaction temperature.

Catalyst Characterization

Chemisorption experiments were carried out in a high-vacuum system by volumetric method. Research grade gases (H_2: 99.9995%, O_2: 99.99%, Takachiho Trading Co., Ltd.) were used without further purification. Before H_2 and

O_2 adsorption measurement, the catalysts, previously reduced in a fixed-bed flow reactor, were treated again in H_2 at 1123 K for 30 min. H_2 adsorption was performed at room temperature, and O_2 consumption was obtained at 873 K. The gas pressure at equilibrium was about 26.3 kPa. The sample weight was about 0.5 g. The dead volume of the apparatus was about 30 cm^3.

RINT 2400 (Rigaku) X-ray diffractometer instrument with monochoromatized CuK_α radiation was used for XRD measurements. The XRD spectra were measured under atmosphere.

The surface area was obtained by the BET method with a Gemini (Micrometrics).

The amount of carbon species formed during CH_4-CO_2 reforming was characterized by temperature-programmed hydrogenation (TPH) as reported previously (29); 0.05 g catalyst was reduced in H_2 flow at 1123 K for 30 min prior to the introduction of reactant gas ($CH_4/CO_2 = 1/1$, W/F = 0.1 gh/mol, 773 K). After the reaction for 2, 30, or 60 min, the feed gas was switched to Ar for 10 min for purging; then the reactor was quickly cooled down to the room temperature. It was exposed to H_2 instead of Ar, and the temperature was raised from room temperature to 1123 K at a heating rate of 20 K/min. CH_4 and CO_2 were detected in the effluent gas when the gas was sometimes sampled and analyzed by a FID gas chromatograph equipped with a methanator; and this CO_2 was due to the desorption of CO_2 adsorbed on the basic sites of the catalyst support during the reaction. The desorption of CO_2 ranged between 470 and 670 K. Only methane was observed except in this temperature range. The signal of CH_4 formation was recorded continuously by the FID without a separating column.

The deposited carbon was also characterized by the CO_2 temperature-programmed reaction (CO_2 TPR). First, CH_4 decomposition was monitored by TG apparatus so that we could obtain the samples with a small amount of deposited carbon (<20 mg C/g-cat). Second, the sample was transferred to the fixed-bed flow reaction system; the samples were heated under CO_2 flow (50 ml/min) from room temperature to 1123 K at a heating rate of 10 K/min; and at 1123 K the temperature was held for 30 min. The FID-GC, equipped with a Porapak Q column and a methanator, was used to analyze the gas product composition. Under the same condition, CO_2 TPR was also performed on the freshly reduced catalysts without exposing the sample to the atmosphere.

Transmission electron microscope (TEM) images were taken by means of a JEM-2020F (JEOL) operated at 200 kV. Samples were dispersed in tetrachloromethane by supersonic waves and put on Cu grids for the TEM observation under atmosphere.

FTIR measurements were carried out in an *in-situ* IR cell combined with a closed circulating system. FTIR spectra were recorded by Magna 550 (Nicolet) in a transmission mode with 2 cm^{-1} resolution using a MCT detector. About 0.15 g of catalyst was pressed into a 20 mmϕ self-supporting disk and put into a slit of the holder in the IR cell. The catalysts were reduced in the IR cell at 1123 K for 0.5 h. CO_2 was introduced into the IR cell at 1.3 kPa for 10 min and evacuated. And then the FTIR spectra of the CO_2 adsorption were measured.

RESULTS AND DISCUSSION

TG Analysis and TEM Observation of Carbon Deposition Behavior

Figures 1a–c show the TG profiles of various catalysts in the CO_2 reforming of CH_4. After a short initial induction period, the sample weight was increased linearly with the time on stream over 3 mol% Ni/MgO and NiO-Al_2O_3 (3 mol%). But no carbon was accumulated on $Ni_{0.03}Mg_{0.97}O$ at 773 K. At higher reaction temperatures, the amount of deposited carbon is decreased, probably because of the equilibrium (3). It was found that $Ni_{0.03}Mg_{0.97}O$ showed excellent resistance to carbon deposition in the CO_2 reforming of methane. The amount of carbon deposition was NiO-Al_2O_3 (3 mol%) > 3 mol% Ni/MgO > $Ni_{0.03}Mg_{0.97}O$ at each reaction temperature.

It is known that CH_4 decomposition and CO disproportionation proceed as side reactions of CO_2 reforming, and these reactions are supposed to be the possible routes for generating deposited carbon. It has been reported that the reactive surface carbon originates from methane and that the less active carbon accumulation follows the catalyst deactivation rate, by ^{13}C labeling studies (30). In contrast, it has been claimed that accumulated carbon species originate from CO_2 (31). The reaction route and the mechanism of carbon deposition during the reforming of CH_4 with CO_2 have not been made clear yet. Therefore, in this study, we observed the TG profiles under CH_4/N_2 and CO/N_2, as illustrated in Fig. 2. Except for NiO-Al_2O_3 (3 mol%) being exposed to CH_4/N_2, the amount of carbon only increased in the early stage of reactions, and then tended to be constant with time on-stream. It has been demonstrated that filamentous carbon was the predominant form of carbon when CH_4 or CO was decomposed below 973 K (20, 21), and it is known that this kind of carbon does not cause catalyst deactivation. In our TEM observation, which will be discussed later, encapsulating carbon was not observed after the reaction. In addition, the gasification of deposited carbon on these catalysts by H_2 or CO_2 has been found to start at 673 K (Fig. 7 and Fig. 8). These suggested that the appearance of a plateau in the TG curves is probably due to reaction equilibrium.

Figure 3 shows the TEM images of $Ni_{0.03}Mg_{0.97}O$ after various treatments. It can be seen that the TEM image after H_2 reduction is very similar to that after CH_4-CO_2

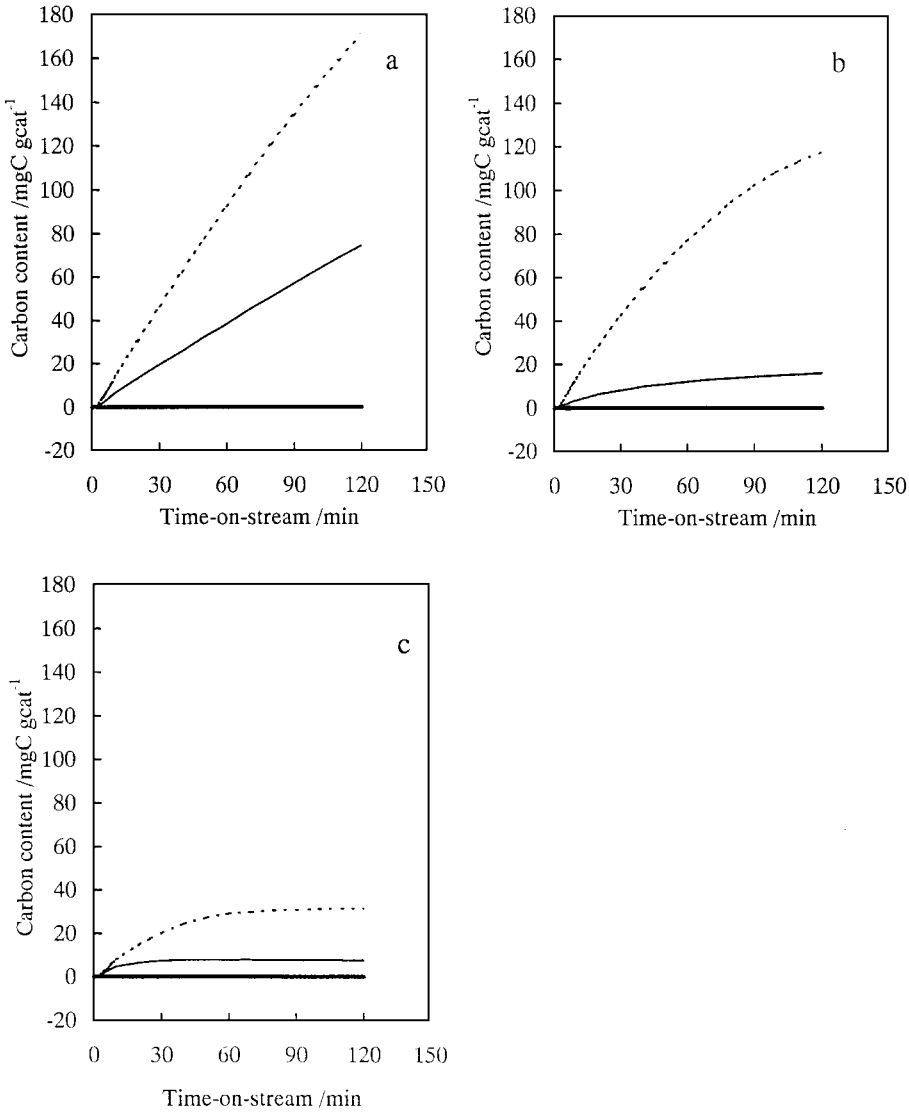

FIG. 1. Carbon content of various catalysts versus time on-stream by TG analysis at (a) 773 K; (b) 973 K; (c) 1123 K, during CH_4-CO_2 reaction. Catalyst: 0.1 g; $CH_4/CO_2/N_2 = 25/25/50$; flow rate: 80 ml/min. $Ni_{0.03}Mg_{0.97}O$ ——; 3 mol% Ni/MgO ——; NiO-Al_2O_3 (3 mol%) - - - -.

reforming at 773 K for 2 h. Only a few small Ni particles are observed from Figs. 3a and b. However, when $Ni_{0.03}Mg_{0.97}O$ was treated in CH_4/N_2 at 773 K for 2 h, a large quantity of whisker carbon appears, with the diameter centered at around 5 nm (Fig. 3c), and most whiskers have a Ni particle at the end. This morphology is quite similar to that reported by Rostrup-Nielsen also under CH_4/N_2 atmosphere (3). The increased weight in TG profiles should be mainly due to whisker carbon growth. Here, we cannot observe the formation of encapsulating carbon. In contrast to CH_4 decomposition, a smaller amount of whisker carbon was formed when the catalyst was treated in CO/N_2. This shows the same tendency as TG results. Whisker carbon from CO disproportionation seems to be thinner than that from CH_4 decomposition. On the other hand, many more Ni particles appeared in the TEM images after CH_4 decomposition and CO disproportionation than those after H_2 reduction and CH_4-CO_2 reforming. As reported previously, the $Ni_{0.03}Mg_{0.97}O$ solid solution catalyst after H_2 reduction had very small Ni particles (<3 nm) (27). TEM results indicate that the aggregation of Ni particles occurred in the process of CH_4 decomposition and CO disproportionation. Considering the thinner whisker carbon from CO disproportionation, CH_4 is suggested to promote Ni aggregation more than CO.

Figure 4 shows TEM images of 3 mol% Ni/MgO after various treatments. On a reduced catalyst there were many Ni particles with a broad size distribution (Fig. 4a). The TEM image changed after CO_2 reforming of CH_4 at 773 K for 2 h (Fig. 4b). Small Ni particles were retained without carbon deposition, but a considerable amount of whisker carbon

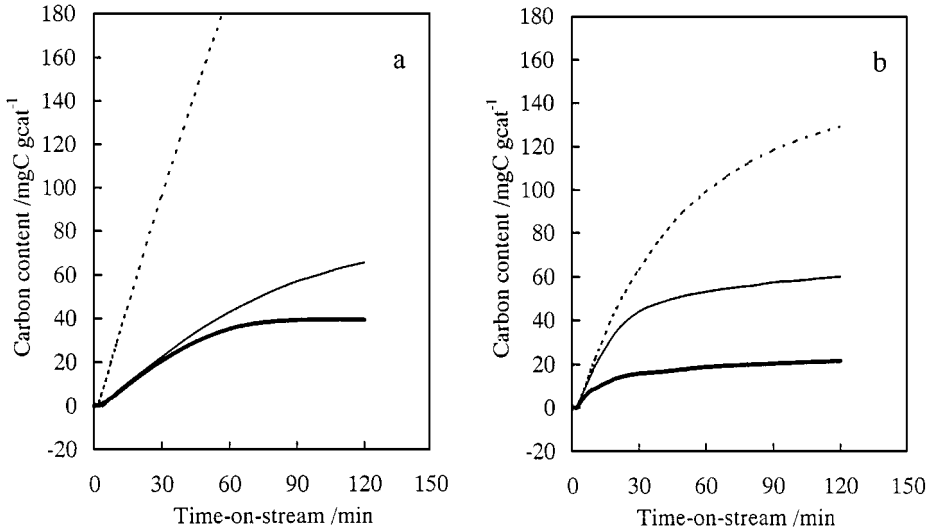

FIG. 2. Carbon content of various catalysts versus time on-stream by TG analysis at 773 K, during methane decomposition and CO disproportionation: (a) $CH_4/N_2 = 25/75$; (b) $CO/N_2 = 25/75$. Catalyst: 0.1 g; flow rate: 80 ml/min. $Ni_{0.03}Mg_{0.97}O$ ——; 3 mol% Ni/MgO ——; NiO-Al_2O_3 (3 mol%) - - - -.

was observed on large Ni particles. The whisker diameter was mostly centered at about 50 nm, and each whisker had a Ni particle standing on the tip. From Fig. 4c, much more whisker carbon was observed after CH_4 decomposition at 773 K for 2 h with the diameters ranging between 5 and 50 nm. Compared with Fig. 4b, the presence of CO_2 was found to be able to extinguish the formation of whisker carbon on small Ni particles. In contrast to CH_4 decomposition, 3 mol% Ni/MgO after CO disproportionation (Fig. 4d) showed a smaller amount of whisker carbon and the diameter of the whiskers was smaller (about 10 nm). This tendency was also observed on $Ni_{0.03}Mg_{0.97}O$.

Figure 5 shows the TEM images of NiO-Al_2O_3 (3 mol%) after various treatments. On a reduced catalyst, Ni particles were difficult to distinguish from the Al_2O_3, due to the amorphous structure of Al_2O_3, as observed by XRD. However, when this catalyst was treated in CH_4/CO_2 at 773 K for 2 h, whisker carbon appeared with diameters ranging between 10 and 25 nm. From Fig. 5c, it can be seen that decomposing CH_4 at 773 K for 2 h led to more whisker carbon with a diameter range of 10–35 nm. This is consistent with the trend of carbon deposition obtained from TG results. Similar to the other catalysts, NiO-Al_2O_3 (3 mol%) also showed a smaller amount of whisker carbon and the smaller diameter (about 15 nm) after CO disproportionation than those after CH_4 decomposition. It is interesting that the morphologies of carbon given by Fig. 5b and Fig. 5c are analogous in diameter distribution and that only a small amount of carbon was decreased by the coexistence of CO_2. In this aspect, NiO-Al_2O_3 (3 mol%) differed significantly from the other catalysts.

Figure 6 shows the initial stage of TG profiles at 773 K and Table 1 gives the initial carbon formation rate. The initial rate was estimated by the rate just after the induction period. In addition, the TOF was based on the amount of H_2 consumption as shown later in Table 2. It is evident that the initial carbon formation rate was obviously decreased by the presence of CO_2, and the difference in the initial carbon formation rate between CH_4 decomposition and the reforming of CH_4 with CO ($\Delta r = r_{(CH4\ decomposition)} - r_{(CO2\ reforming\ of\ CH4)}$) was dependent on the catalysts and the order was as follows: $Ni_{0.03}Mg_{0.97}O$ > 3 mol% Ni/MgO > NiO-Al_2O_3 (3 mol%).

TABLE 1

The Rate of Carbon Formation due to CO_2 Reforming, CH_4 Decomposition, and CO Disproportionation

Catalyst	Temp.[a]/K	TOF/s^{-1} reaction			Δr^e/s^{-1}
		CH_4-CO_2[b]	CH_4[c]	CO[d]	
$Ni_{0.03}Mg_{0.97}O$	773	0	0.11	0.26	≥0.11
	973	0	0.19	0.03	≥0.19
	1123	0	0.46	0	≥0.46
3 mol% Ni/MgO	773	0.07	0.13	0.17	0.06
	973	0.04	0.19	0.19	0.15
	1123	0.08	0.27	0.04	0.19
NiO-Al_2O_3 (3 mol% Ni)	773	0.08	0.16	0.13	0.08
	973	0.08	0.10	0.06	0.02
	1123	0.04	0.06	0	0.02

Note. TOF was based on H_2 consumption in Table 2.
[a] Reaction temperature.
[b] $CH_4/CO_2/N_2 = 25/25/50$, total flow rate: 80 ml/min, 0.1 g catalyst.
[c] $CH_4/N_2 = 25/75$, total flow rate: 80 ml/min, 0.1 g catalyst.
[d] $CO/N_2 = 25/75$, total flow rate: 80 ml/min, 0.1 g catalyst.
[e] The rate difference between r CH_4 and $r$$CH_4$-$CO_2$.

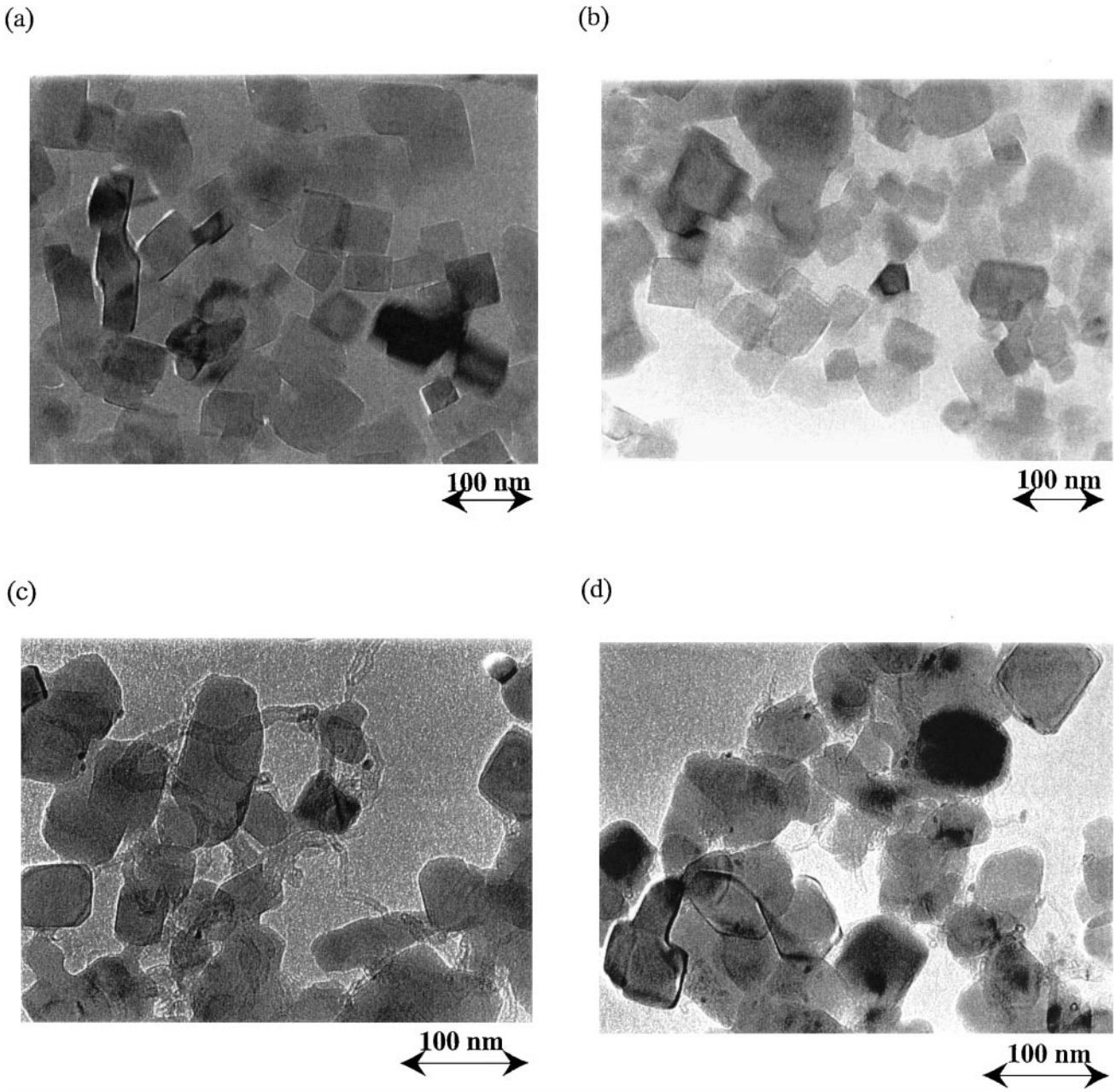

FIG. 3. TEM images of $Ni_{0.03}Mg_{0.97}O$ solid solution catalyst after H_2, $CH_4/CO_2/N_2$, CH_4/N_2, and CO/N_2 treatment: (a) H_2 reduction at 1123 K for 30 min; (b) $CH_4/CO_2/N_2 = 25/25/50$, 773 K; (c) $CH_4/N_2 = 25/75$, 773 K; (d) $CO/N_2 = 25/75$, 773 K. Total flow rate 80 ml/min; reaction time 2 h.

This indicated that CO_2 plays an important role in inhibiting carbon deposition. Therefore, we investigated the interaction between CO_2 and the catalyst surface, as discussed below. The addition of basic oxides to Ni/Al_2O_3 suppressed carbon deposition in methane decomposition as well as the CO_2 reforming of methane (32). But in our case, the carbon deposition rate in methane decomposition was almost the same on $Ni_{0.03}Mg_{0.97}O$ and 3 mol% Ni/MgO, while that in CO_2 reforming of methane was much different.

Catalyst Characterization and the Interaction between CO_2 and the Catalyst Surface

Table 2 lists some characteristic properties of catalysts after H_2 reduction. The BET surface area of $Ni_{0.03}Mg_{0.97}O$ and Ni/MgO was almost the same. On the other hand, that of $NiO\text{-}Al_2O_3$ (3 mol%) was much larger. According of XRD analysis, the XRD pattern of reduced $NiO\text{-}Al_2O_3$ (3 mol%) coincided well with that of $\gamma\text{-}Al_2O_3$. Broad XRD

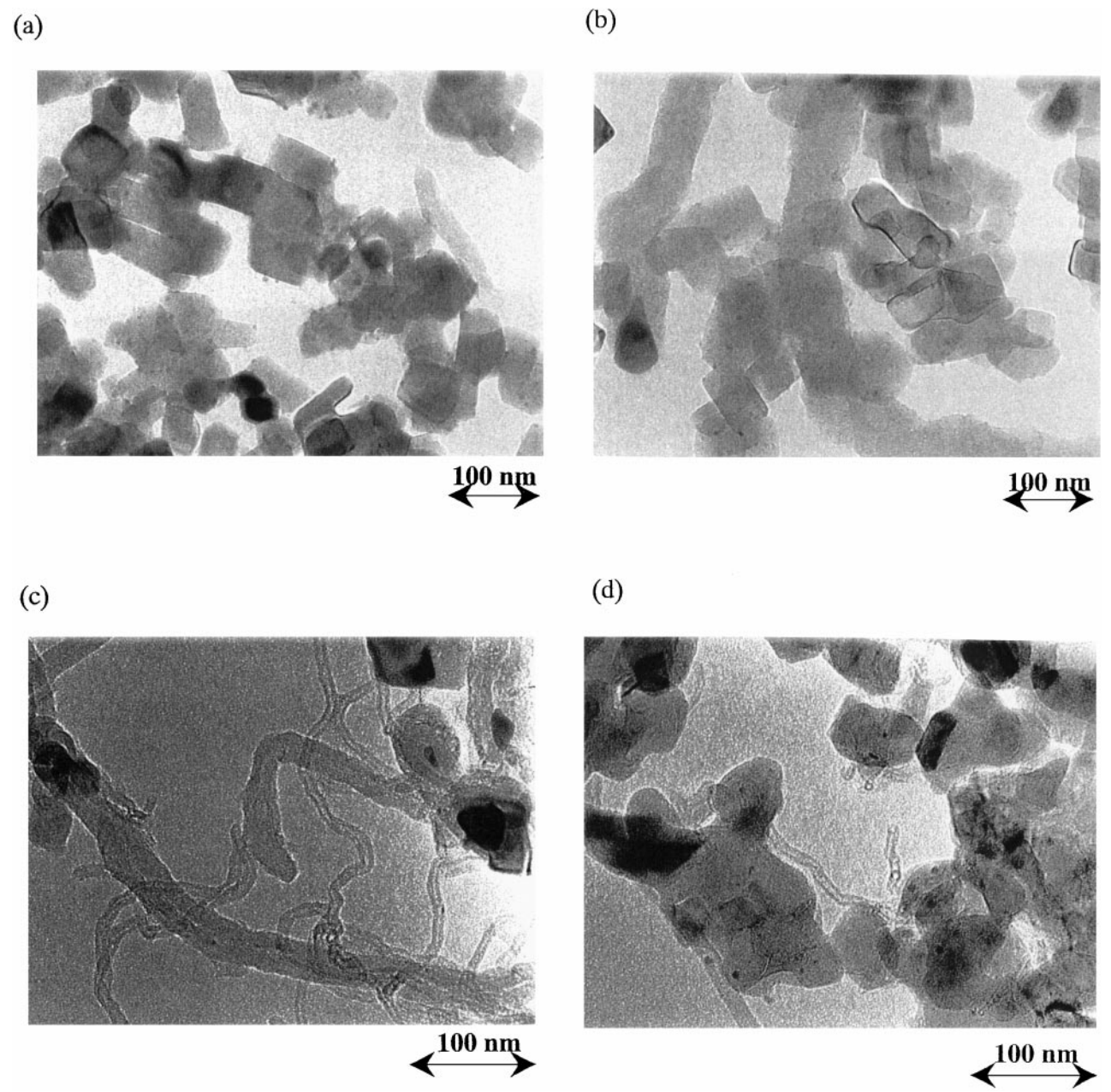

FIG. 4. TEM images of 3 mol% Ni/MgO catalyst after H_2, CH_4/CO_2, CH_4/N_2, and CO/N_2 treatment: (a) H_2 reduction at 1123 K for 30 min; (b) $CH_4/CO_2/N_2 = 25/25/50$, 773 K; (c) $CH_4/N_2 = 25/75$, 773 K; (d) $CO/N_2 = 25/75$, 773 K. Total flow rate 80 ml/min; reaction time 2 h.

peaks at $2\theta = 45.79^\circ$ and 67.03° were observed. More amorphous structure of this catalyst corresponded well to the high BET surface area. And generally, Ni^{2+} ions react with alumina to form $NiAl_2O_4$ spinel-type oxide (33). But in this case, the XRD pattern of spinel compound was not observed, probably due to the low Ni content. In addition, the peak of Ni metal was not observed, either. The position of the highest XRD peak on reduced $Ni_{0.03}Mg_{0.97}O$ was $2\theta = 42.93^\circ$. XRD patterns of $Ni_{0.03}Mg_{0.97}O$ before and after reduction pretreatment were just the same. This indicated that the bulk structure of the solid solution was maintained even after H_2 reduction. In addition, the lattice constant determined by XRD is satisfied with the relation between the Ni content in the nickel magnesia solid solution and the lattice constant as reported (34). On 3 mol% Ni/MgO a small peak ($2\theta = 44.5^\circ$) which can be assigned to the Ni metal was observed. This indicated that there are large Ni particles on this supported catalyst. A strong peak at $2\theta = 42.90^\circ$ with a shoulder at $2\theta = 43.02^\circ$ was observed. The main peak can be assigned to MgO and the shoulder

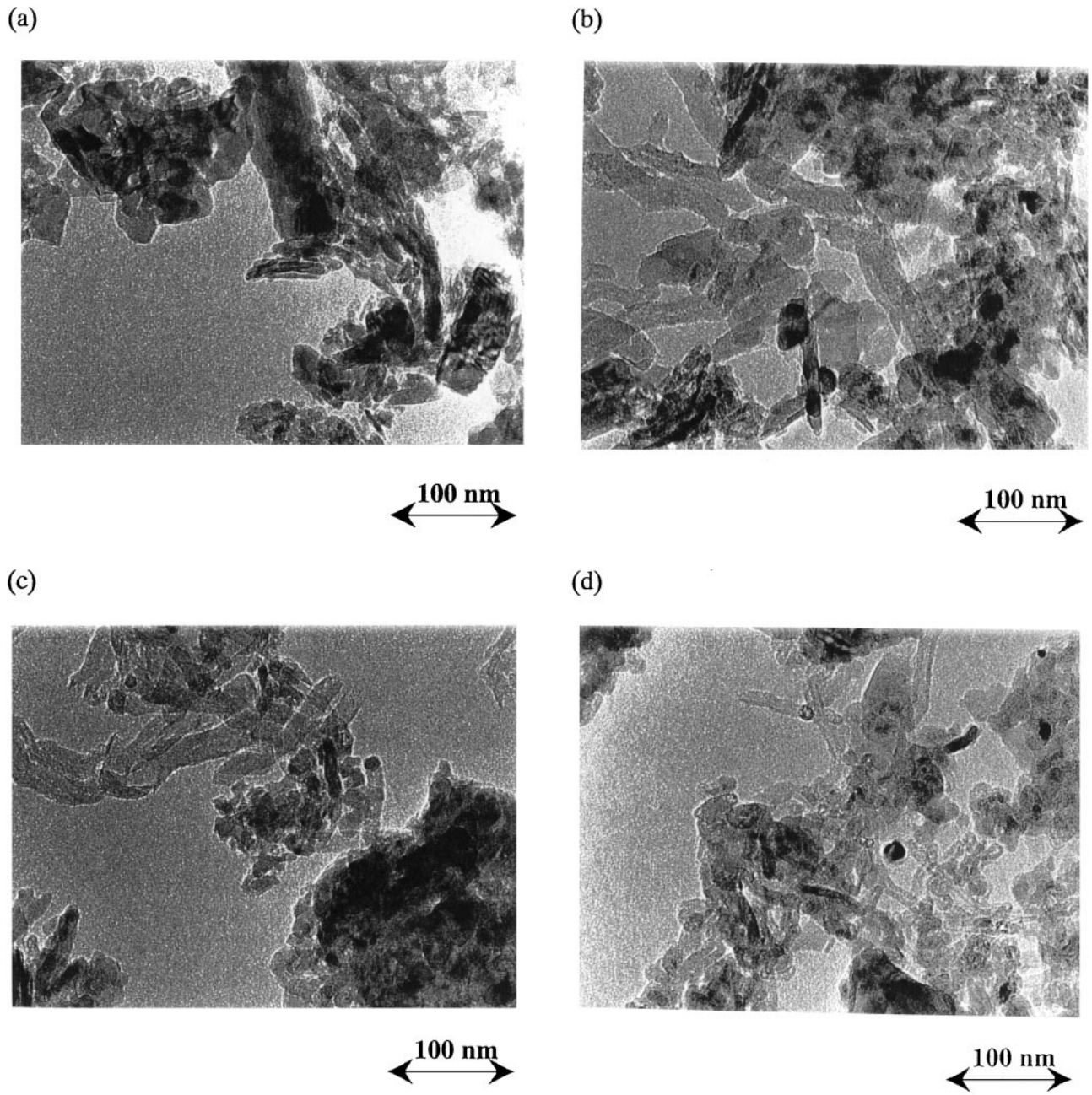

FIG. 5. TEM images of NiO-Al_2O_3 (3 mol%) catalyst after H_2, CH_4/CO_2, CH_4/N_2, and CO/N_2 treatment: (a) H_2 reduction at 1123 K for 30 min; (b) $CH_4/CO_2/N_2 = 25/25/50$, 773 K; (c) $CH_4/N_2 = 25/75$, 773 K; (d) $CO/N_2 = 25/75$, 773 K. Total flow rate 80 ml/min; reaction time 2 h.

can be assigned to the solid solution with high Ni content. The content is determined to be about $Ni/(Ni + Mg) = 0.3$, using the relation described in Ref. (34). This indicated that three phases are present at least: large nickel particle; MgO; nickel magnesia solid solution with high Ni content.

The degree of reduction (the ratio of reduced Ni to total Ni) is estimated by O_2 consumption at 873 K, based on assuming that $Ni^0 + 1/2O_2 \rightarrow NiO$. Since a part of the O_2 can be consumed by the oxide support, this assumption is not accurate, but qualitative interpretation is thought to be possible. The reducibility of $Ni_{0.03}Mg_{0.97}O$ was very low, and the reduction degree of Ni was at most 3%, indicating that the Ni^{2+} in this nickel magnesia solid solution is very difficult to reduce. This agrees with the result reported by Parmaliana *et al.* that the formation of NiO-MgO solid solution lowered the reducibility of Ni^{2+} and this phenomenon was particularly remarkable for the solid solution with low

TABLE 2

Catalyst Properties

Catalyst	Amount of consumption		$2 \times O_2/Ni_{total}$[c]	H_2/O_2[d]	BET/	r_{CO}[e]/	TOF[f]/s^{-1}	Amount of carbon[g]/
	H_2[a]	O_2[b]/μmol g^{-1}	%[c]	%[d]	m^2 g^{-1}	μmol g^{-1} s^{-1}		mgC g cat^{-1}
$Ni_{0.03}Mg_{0.97}O$	3.1	10.5	2.9	29.5	19	40	6.5	0.5
3.0 mol% Ni/MgO	3.9	226.5	62.4	1.7	16	160	20.5	6.0
NiO-Al_2O_3 (3.0 mol% Ni)	7.6	78.0	27.0	9.7	85	166	10.9	57.4

[a] 298 K.
[b] 873 K.
[c] 2 × (Amount of O_2 consumption)/(Total amount of Ni in catalyst).
[d] (Amount of H_2 consumption)/(Amount of O_2 consumption).
[e] Reaction condition: 0.1 MPa, $CH_4/CO_2 = 1$, 773 K, W/F = 0.1 gh/mol.
[f] TOF was based on the amount of H_2 consumption.
[g] Amount of β-carbon after 1 h of reforming reaction; the reaction condition is the same as *e*).

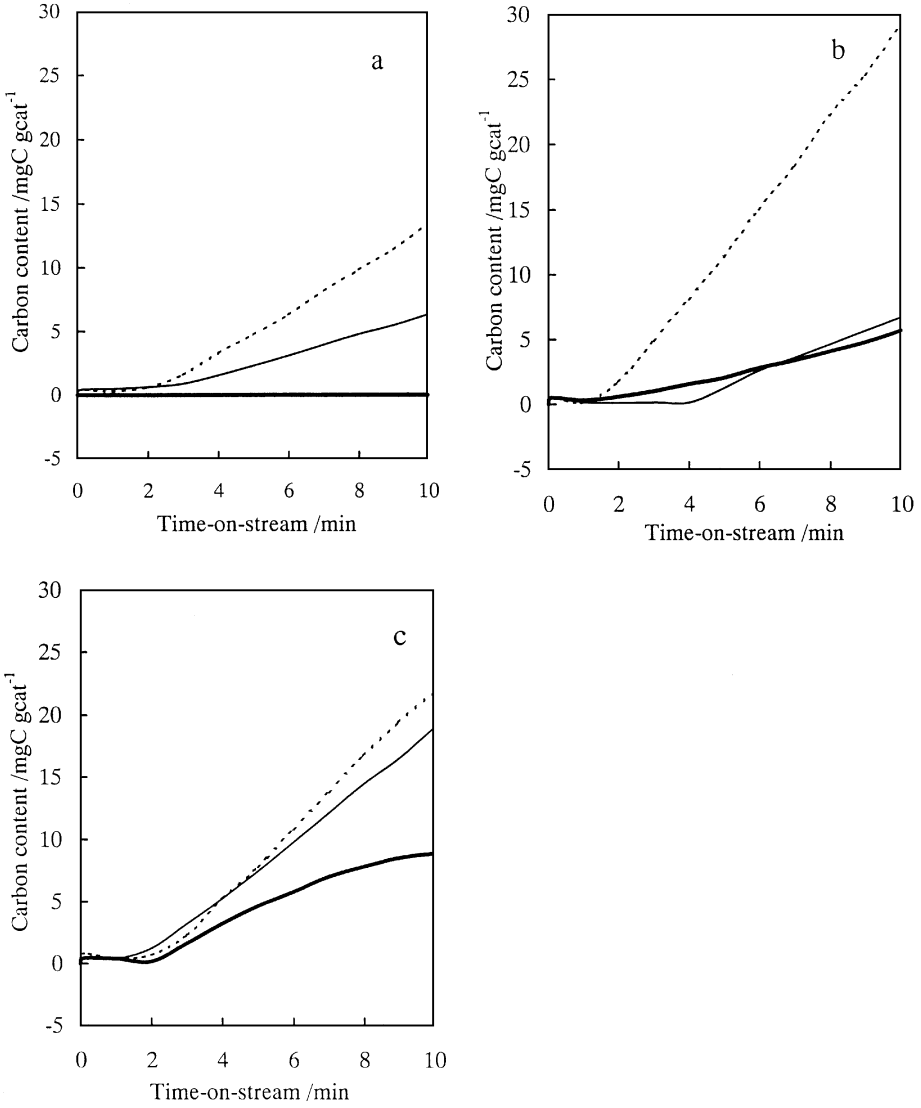

FIG. 6. Initial carbon deposition on various catalysts in (a) CH_4-CO_2 reaction; (b) CH_4 decomposition; and (c) CO disproportionation at 773 K by TG analysis. Catalyst: 0.1 g; flow rate: 80 ml/min. Partial pressure: $CH_4/CO_2/N_2 = 25/25/50$; $CH_4/N_2 = 25/75$; or $CO/N_2 = 25/75$. $Ni_{0.03}Mg_{0.97}O$ ——; 3 mol% Ni/MgO ——; NiO-Al_2O_3 (3 mol%) - - - -.

Ni content (35). In the case of 3 mol% Ni/MgO under the same condition, about 62% of the nickel underwent reduction. This fact means that a considerable part of the nickel was irreducible under the present reduction condition. It suggests the dissolution of a part of the nickel into the MgO lattice. This is consistent with XRD analysis. In addition, it is noteworthy that NiO-Al_2O_3 (3 mol%) has a 9 times higher ratio of O_2 consumption than $Ni_{0.03}Mg_{0.97}O$, while it has only a 4 times higher BET surface area. Ni^{2+} ions in NiO-Al_2O_3 (3 mol%) is not as difficult to reduce as those in the $Ni_{0.03}Mg_{0.97}O$ solid solution.

The number of surface Ni atoms in reduced Ni metal can be estimated by H_2 adsorption at room temperature on the basis of $H/Ni^0_{surf} = 1$. It is thought that the dispersion of Ni particles can be expected by (the number of surface Ni atoms obtained from H_2 consumption)/(the number of reduced Ni atoms obtained from O_2 consumption). As demonstrated in Table 2, this ratio (H_2/O_2) among these catalysts is in the order of $Ni_{0.03}Mg_{0.97}O$ > NiO-Al_2O_3 (3 mol%) > 3 mol% Ni/MgO. This result is consistent with XRD results that the signal attributed to Ni metal was observed on 3 mol% Ni/MgO, but the signal was not observed at all on $Ni_{0.03}Mg_{0.97}O$ and NiO-Al_2O_3 (3 mol%). TOF is estimated by CO formation rate and H_2 consumption. The order of TOF is as follows: 3 mol% Ni/MgO > NiO-Al_2O_3 (3 mol%) > $Ni_{0.03}Mg_{0.97}O$. Methane conversion was 2.1%, 8.2%, and 8.4% on $Ni_{0.03}Mg_{0.97}O$, 3 mol% Ni/MgO, and NiO-Al_2O_3 (3 mol%), respectively. The order of TOF is reversed for the H_2/O_2 ratio in Table 2. The activity seems to be higher on larger Ni particles.

The amount of deposited carbon was estimated by the temperature-programmed hydrogenation method (TPH). TPH results are shown in Fig. 7. In TPH profiles, two peaks of methane formation were observed. As reported before (29), the peak at 550–700 K (α-carbon) was mainly attributed to hydrogenation of CO_2 adsorbed on the support surface. The reactive carbon species on noble metal catalysts has been reported (36). The reactivity in TPH may not be so different, but in our result the amount of α-carbon was much larger than the number of surface nickel atoms estimated by the H_2 consumption listed in Table 2. Therefore, α-carbon can not be assigned to the reactive carbon species on a metal surface as reported previously (29). On the other hand, the peak above about 750 K (β-carbon) was attributed to the hydrogenation of deposited carbon. The amount of β-carbon formed during 60 min of reaction was summarized in Table 2. The order of carbon amount is NiO-Al_2O_3 (3 mol%) > 3 mol% Ni/MgO $\gg$ $Ni_{0.03}Mg_{0.97}O$. This order agrees with TGA results. But this order is different from that of the H_2/O_2 ratio and CO formation rate. It is found that carbon deposition does not have a direct relation to the catalytic activity. This indicates that the selectivity of carbon formation must be different on each catalyst. It is known that basic additive decreased carbon deposition in methane reforming (32). Support basicity is thought to have an effect on the order of carbon amount on these three catalysts.

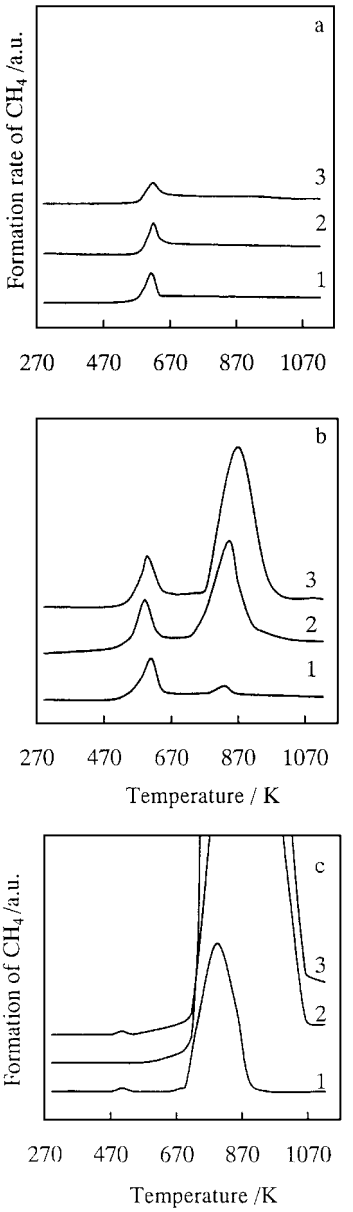

FIG. 7. Profiles of temperature programmed hydrogenation on (a) $Ni_{0.03}Mg_{0.97}O$; (b) 3 mol% Ni/MgO; and (c) NiO-Al_2O_3 (3 mol%) catalysts after CH_4-CO_2 reforming reaction at 773 K for (1) 2 min, (2) 30 min, and (3) 60 min. Reaction condition: $CH_4/CO_2 = 1/1$; 0.1 MPa; W/F = 0.1 gh/mol; catalyst weight: 0.05 g. TPH condition: 100% H_2; flow rate: 50 ml/min; 0.1 MPa; heating rate: 20 K/min.

The reactivity of carbon with CO_2 was investigated by means of CO_2 TPR (Figs. 8a, b). CO_2 TPR profiles were also obtained on freshly reduced catalyst (Fig. 8c). At this moment, the assignment of all TPR peaks is difficult, but it may be deduced that the peaks in 673–873 K and about 1073 K may be attributed to the deposited carbon. However,

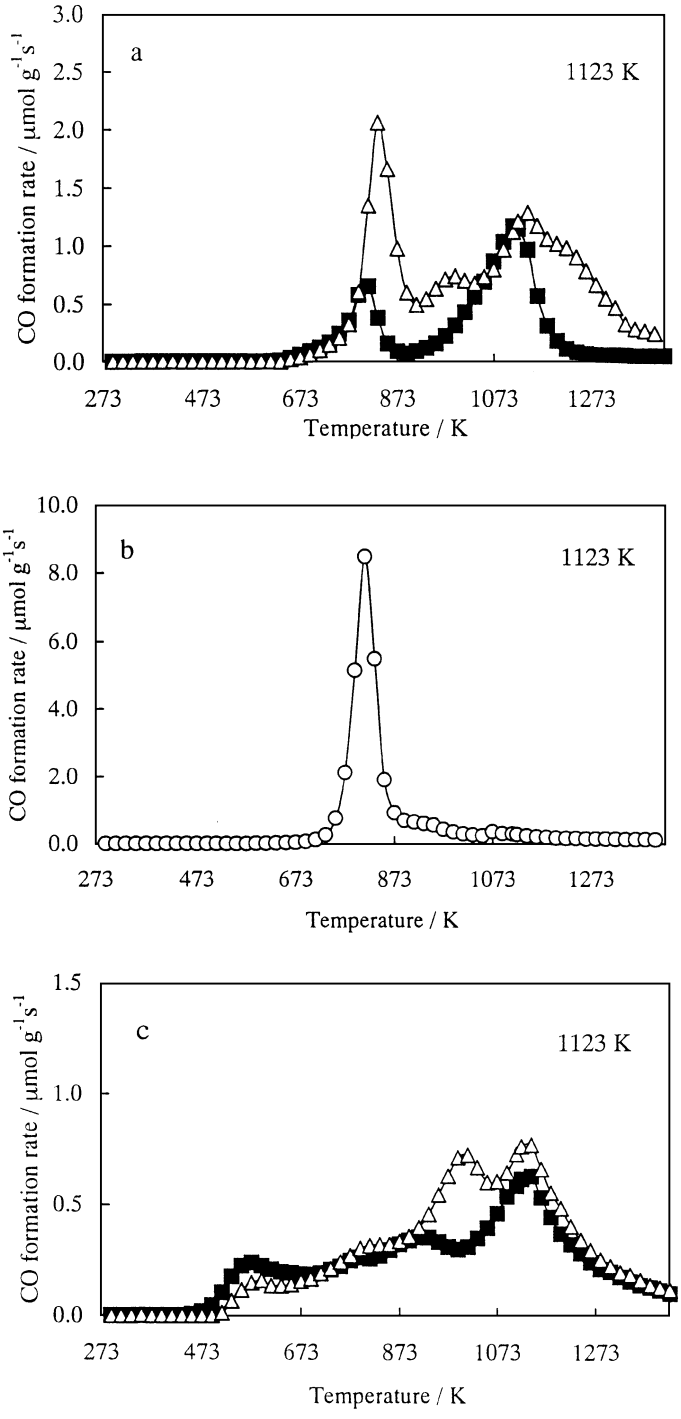

FIG. 8. Profiles of temperature-programmed reaction of CO_2 obtained over $Ni_{0.03}Mg_{0.97}O$, 3 mol% Ni/MgO, and NiO-Al_2O_3 (3 mol%): (a) $Ni_{0.03}Mg_{0.97}O$ (■), 3 mol% Ni/MgO (△) after treatment in CH_4/N_2 at 773 K; (b) NiO-Al_2O_3 (3 mol%) (○) after treatment in CH_4/N_2 at 773 K; (c) $Ni_{0.03}Mg_{0.97}O$ (■), 3 mol% Ni/MgO (△) after H_2 reduction at 1123 K for 30 min. 0.1 g catalyst, $CH_4/N_2 = 25/75$, 773 K, total flow rate: 80 ml/min; CO_2-TPR: flow rate 50 ml/min, 298–1123 K, 10 K/min.

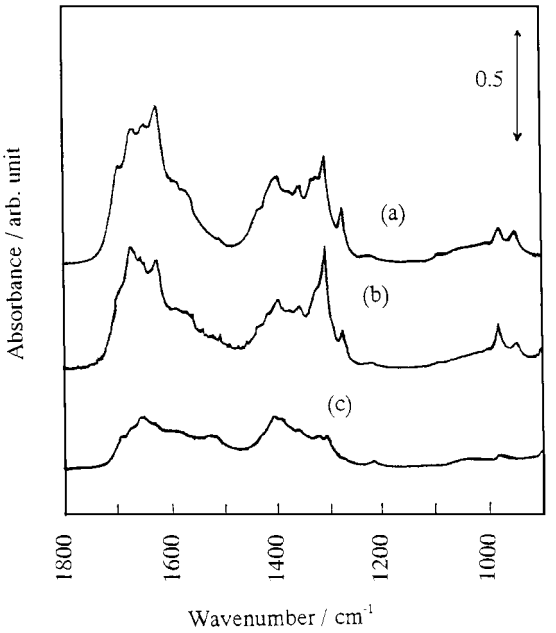

FIG. 9. FTIR spectra of CO_2 adsorption on (a) MgO, (b) $Ni_{0.03}Mg_{0.97}O$, (c) 3 mol% Ni/MgO after H_2 reduction at 1123 K for 30 min. Pressure of CO_2 exposure: 1.3 kPa; adsorption and evacuation at 298 K.

the peak above 1073 K was also observed in Fig. 8c. This peak (about 1073 K) in CO_2 TPR profiles is not responsible for the deposited carbon, it may be derived from the support; while the peak in 673–873 K can be assigned to the deposited carbon. It is noted that for all these catalysts, the maximum peak temperature is located at 817–837 K. This means that the reactivity of carbon with CO_2 on each catalyst is almost the same. From the TPH results, the reactivity of deposited carbon toward hydrogen was almost the same on 3 mol% Ni/MgO and NiO-Al_2O_3 (3 mol%). From the fact that our TG and TEM results demonstrated the large difference in the anticoking performance of these catalysts when CO_2 coexists with CH_4, the different behavior of carbon deposition seems to be caused by inhibiting the formation of carbon precursor. Furthermore, it is found that $Ni_{0.03}Mg_{0.97}O$ was more active for CO_2 dissociation than 3 mol% Ni/MgO in profiles of CO_2 TPR. The starting temperature of CO formation is decreased by 20 K on $Ni_{0.03}Mg_{0.97}O$ (Fig. 8c). The interaction of CO_2 with reduced catalyst is different between $Ni_{0.03}Mg_{0.97}O$ and 3 mol% Ni/MgO. Then we investigated this interaction by FTIR of CO_2 adsorption.

Figure 9 shows the FTIR spectra of CO_2 adsorption on MgO, $Ni_{0.03}Mg_{0.97}O$, and 3 mol% Ni/MgO reduced at 1123 K for 30 min. CO_2 adsorption on $Ni_{0.03}Mg_{0.97}O$ catalyst was very similar to that on MgO. Two kinds of bidentate carbonate (1670/1305 and 1625/1272 cm^{-1}) and one kind of bicarbonate (1652/1405 cm^{-1}) were observed. Peak assignment was referred to some papers (37–39). On the $Ni_{0.03}Mg_{0.97}O$

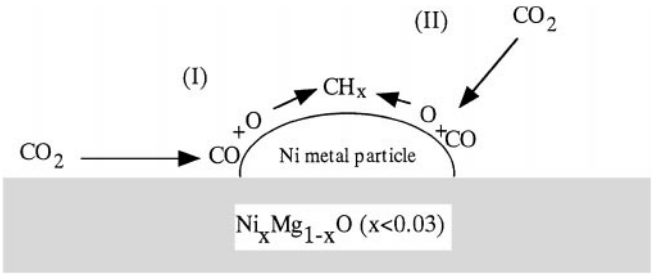

FIG. 10. Model of the reaction scheme of CH_x adsorbed on nickel metal surface with CO_2 in CO_2 reforming of methane.

catalyst more bidentate carbonate was observed. In contrast, on the 3 mol% Ni/MgO catalyst, more bicarbonate was observed; the 3 mol% Ni/MgO was much different from MgO in terms of CO_2 adsorption. This is probably due to the formation of solid solution near the surface of the MgO support, which is suggested by the oxygen consumption and the XRD analysis. In this case, the concentration of surface Ni ion may be much higher than that of $Ni_{0.03}Mg_{0.97}O$; 3 mol% Ni/MgO has different surface properties of support than $Ni_{0.03}Mg_{0.97}O$.

It has been reported that surface properties have a great effect on the carbon deposition. Carbon deposition in both CO_2 reforming of methane and methane decomposition has been reported to be highly suppressed by adding basic metal oxides to Ni/Al_2O_3 (32). Support oxides have been reported to play an important role in the inhibition of carbon deposition during CO_2 reforming of methane on Ni/La_2O_3 (40, 41). The origin and the reactivity of carbonaceous species accumulated during reaction are found to depend strongly on the support composition in $Ni/CaO\text{-}Al_2O_3$ (42).

Figure 10 shows the inhibition mechanism of carbon deposition on $Ni_{0.03}Mg_{0.97}O$. It can be considered that, in the case of $Ni_{0.03}Mg_{0.97}O$, at first the active carbon species (CH_x) is formed on the nickel metal surface via the activation of CH_4, and this can be removed rapidly before converting to whisker carbon. On the contrary, on other catalysts, the formation of CH_x and its transformation to whisker carbon may become faster than the removal by H_2 or CO_2 etc. As a consequence, the concentration of CH_x species may be higher, and a part of them can be converted to a carbon precursor, or a surface carbide before reacting with CO_2. There are two paths for the reaction of carbon species on Ni with CO_2 as shown in Fig. 10. The one is CO_2 adsorbed on Ni and the other is CO_2 adsorbed on the surface of support. It is known that CO_2 can adsorb on a Ni metal surface from the gas phase and dissociate to oxygen and CO (Fig. 10(II)). Reduced $Ni_{0.03}Mg_{0.97}O$ is basic on its surface and interacts strongly with CO_2, like MgO. Therefore, CO_2 can be activated easily at the interface between reduced Ni and the solid solution surface, similar to MgO (Fig. 10(I)). Reaction path I is the main one in the case of small nickel particles, and reaction path II is the main one in the case of large nickel particles. The fact that carbon was deposited on large nickel particles on 3 mol% Ni/MgO indicated that path I is very imporatant in the inhibition of carbon deposition. This is intimately related to the high resistance to carbon deposition on $Ni_{0.03}Mg_{0.97}O$ which had small Ni particles interacting with the support surface.

CONCLUSIONS

(1) The $Ni_{0.03}Mg_{0.97}O$ solid solution catalyst had very high resistance to carbon deposition during CO_2 reforming of CH_4 at 773–1123 K.

(2) The $NiO\text{-}Al_2O_3$ (3 mol%) catalyst showed the highest carbon formation among the catalysts studied, indicating that the property of support exerts a strong effect on the anticoking performance of catalyst.

(3) The diameter of whisker carbon formed via CH_4 decomposition was greater than that via CO disproportionation. It suggests that CH_4 promoted the aggregation of nickel more drastically than CO.

(4) In CO_2 reforming of CH_4 on 3 mol% Ni/MgO, carbon was deposited on larger Ni particles and not on small Ni particles.

(5) The order of inhibition of carbon deposition by CO_2 was $Ni_{0.03}Mg_{0.97}O > 3$ mol% $Ni/MgO > NiO\text{-}Al_2O_3$ (3 mol%). This indicated that CO_2 played a more important role in inhibiting carbon deposition on the more basic support.

(6) On reduced $Ni_{0.03}Mg_{0.97}O$ catalyst CO_2 dissociated more easily than on 3 mol% Ni/MgO. This corresponded to the performance of inhibition of carbon deposition and suggested that the inhibition mechanism is caused by the activation of CO_2 at the interface between the metal and the support.

ACKNOWLEDGMENTS

A part of this research was supported by the Proposal-Based New Industry Creative Type Technology R&D Promotion Program from the New Energy and Industrial Technology Development Organization (NEDO) of Japan.

REFERENCES

1. Delmon, B., *Appl. Catal. B* **1**, 139 (1992).
2. Fujimoto, K., *Stud. Surf. Sci. Catal.* **81**, 73 (1994).
3. Rostrup-Nielsen, J. R., *in* "Catalysis Science and Technology" (J. R. Anderson and M. Boudart, Eds.), Vol. 5. Springer-Verlag, New York, 1984.
4. *Oil and Gas J.* Nov. 21, p. 30 (1994), as an example.
5. Gadalla, A. M., and Bower, B., *Chem. Eng. Sci.* **43**, 3049 (1988).
6. Gadalla, A. M., and Sommer, M. E., *Chem. Eng. Sci.* **44**, 2825 (1989).
7. Gadalla, A. M., and Sommer, M. E., *J. Am. Ceram. Soc.* **72**, 683 (1989).
8. Rostrup-Nielsen, J. R., and Hansen, J.-H. B., *J. Catal.* **144**, 38 (1993).

9. Erdohelyi, A., Cserenyi, J., and Solymosi, F., *J. Catal.* **141**, 287 (1993).
10. Tokunaga, O., Osada, Y., and Ogasawara, S., *Fuel* **68**, 990 (1989).
11. Richardson, J. T., and Paripatyadar, S. A., *Appl. Catal.* **61**, 293 (1990).
12. Chubb, T. A., *Sol. Energy* **24**, 341 (1980).
13. McCrary, J., McCrary, G. E., Chubb, T. A., Nemecek, J. J., and Simmons, D. E., *Sol. Energy* **29**, 141 (1982).
14. Fish, J. D., and Hawn, D. C., *J. Sol. Energy Eng.* **109**, 215 (1987).
15. Perera, J. S. H. Q., Couves, J. W., Sankar, G., and Thomas, J. M., *Catal. Lett.* **11**, 219 (1991).
16. Mark, M. F., and Maier, M. F., *J. Catal.* **164**, 122 (1996).
17. Kroll, V. C. H., Swaan, H. M., and Mirodatos, C., *J. Catal.* **161**, 409 (1996).
18. Kim, G. J., Cho, D. S., Kim, K. H., and Kim, J. H., *Catal. Lett.* **28**, 41 (1994).
19. Ashcroft, A. T., Cheetham, A. K., Green, M. L. H., and Vernon, P. D. F., *Nature* **352**, 225 (1991).
20. Bartholomew, C. H., *Catal. Rev. Sci. Eng.* **24**, 67 (1982).
21. Trimm, D. L., *Catal. Rev. Sci. Eng.* **16**, 155 (1977).
22. Yamazaki, O., Nozaki, T., Omata, K., and Fujimoto, K., *Chem. Lett.*, 1953 (1992).
23. Zhang, Z., and Verkyios, X. E., *Catal. Today* **21**, 589 (1994).
24. Zhang, Z., and Verkyios, X. E., *J. Chem. Soc., Chem. Commun.*, 71 (1995).
25. Fujimoto, K., Omata, K., Nozaki, T., Yamazaki, O., and Han, Y., *Energy Convers. Mgmt.* **3**, 529 (1992).
26. Yamazaki, O., Tomishige, K., and Fujimoto, K., *Appl. Catal. A: General* **136**, 49 (1996).
27. Chen, Y. G., Tomishige, K., Yokoyama, K., and Fujimoto, K., *Appl. Catal. A: General* **165**, 335 (1997).
28. Chen, Y. G., Tomishige, K., and Fujimoto, K., *Chem. Lett.*, 999 (1997).
29. Chen, Y. G., Tomishige, K., and Fujimoto, K., *Appl. Catal. A: General* **161**, L11 (1997).
30. Swaan, H. M., Kroll, V. C. H., Martin, G. A., and Mirodatos, C., *Catal. Today* **21**, 571 (1994).
31. Tsipouriari, V. A., Efstathiou, A. M., Zhang, Z. L., and Verykios, X. E., *Catal. Today* **21**, 579 (1994).
32. Horiuchi, T., Sakuma, K., Fukui, T., Kubo, Y., Osaki, T., and Mori, T., *Appl. Catal. A: General* **144**, 111 (1996).
33. Chen, Y. G., and Ren, J., *Catal. Lett.* **29**, 39 (1994).
34. Kale, G. M., *J. Am. Ceram. Soc.* **74**, 2209 (1991).
35. Parmaliana, A., Arena, F., Frusteri, F., and Giordano, N., *J. Chem. Soc., Faraday Trans.* **86**, 2663 (1990).
36. Mark, M. F., and Maier, W. F., *Angew. Chem. Int. Ed. Engl.* **33**, 1657 (1994).
37. Fukuda, Y., and Tanabe, K., *Bull. Chem. Soc. Jpn* **46**, 1616 (1973).
38. Lercher, J. A., Colombier, C., and Noller, H., *J. Chem. Soc., Faraday Trans. 1* **80**, 949 (1984).
39. Philipp, R., and Fujimoto, K., *J. Phys. Chem.* **96**, 9035 (1992).
40. Slagtern, A., Schuurman, Y., Leclercq, C., Verykios, X., and Mirodatos, C., *J. Catal.* **172**, 118 (1997).
41. Zhang, Z., Verykios, V. E., MacDonald, S. M., and Affrossman, S., *J. Phys. Chem.* **100**, 744 (1996).
42. Goula, M. A., Lemonidou, A. A., and Efstathiou, A. M., *J. Catal.* **161**, 626 (1996).